

See discussions, stats, and author profiles for this publication at: <https://www.researchgate.net/publication/258177280>

# Experiments and zero D modeling studies using specific Wiebe coefficients for producer gas as fuel in spark-ignited engines

**Article** in ARCHIVE Proceedings of the Institution of Mechanical Engineers Part C Journal of Mechanical Engineering Science 1989-1996 (vols 203-210) · March 2013

Impact Factor: 0.56 · DOI: 10.1177/0954406212463846

---

CITATIONS

6

---

READS

31

## 2 authors:



**Anand Shivapuji**

Indian Institute of Science

13 PUBLICATIONS 20 CITATIONS

SEE PROFILE



**Dasappa S.**

Indian Institute of Science

114 PUBLICATIONS 920 CITATIONS

SEE PROFILE

# Experiments and zero D modeling studies using specific Wiebe coefficients for producer gas as fuel in spark-ignited engines

Proc IMechE Part C:  
J Mechanical Engineering Science  
227(3) 504–519  
© IMechE 2012  
Reprints and permissions:  
sagepub.co.uk/journalsPermissions.nav  
DOI: 10.1177/0954406212463846  
pic.sagepub.com



Anand M Shivapuji and S Dasappa

## Abstract

The paper addresses experiments and modeling studies on the use of producer gas, a bio-derived low energy content fuel in a spark-ignited engine. Producer gas, generated in situ, has thermo-physical properties different from those of fossil fuel(s). Experiments on naturally aspirated and turbo-charged engine operation and subsequent analysis of the cylinder pressure traces reveal significant differences in the heat release pattern within the cylinder compared with a typical fossil fuel. The heat release patterns for gasoline and producer gas compare well in the initial 50% but beyond this, producer gas combustion tends to be sluggish leading to an overall increase in the combustion duration. This is rather unexpected considering that producer gas with nearly 20% hydrogen has higher flame speeds than gasoline. The influence of hydrogen on the initial flame kernel development period and the combustion duration and hence on the overall heat release pattern is addressed. The significant deviations in the heat release profiles between conventional fuels and producer gas necessitates the estimation of producer gas-specific Wiebe coefficients. The experimental heat release profiles are used for estimating the Wiebe coefficients. Experimental evidence of lower fuel conversion efficiency based on the chemical and thermal analysis of the engine exhaust gas is used to arrive at the Wiebe coefficients. The efficiency factor  $a$  is found to be 2.4 while the shape factor  $m$  is estimated at 0.7 for 2% to 90% burn duration. The standard Wiebe coefficients for conventional fuels and fuel-specific coefficients for producer gas are used in a zero D model to predict the performance of a 6-cylinder gas engine under naturally aspirated and turbo-charged conditions. While simulation results with standard Wiebe coefficients result in excessive deviations from the experimental results, excellent match is observed when producer gas-specific coefficients are used. Predictions using the same coefficients on a 3-cylinder gas engine having different geometry and compression ratio(s) indicate close match with the experimental traces highlighting the versatility of the coefficients.

## Keywords

Alternative fuel, producer gas, zero D modeling, Wiebe coefficients, combustion phasing

Date received: 3 August 2012; accepted: 17 September 2012

## Introduction

Mathematical modeling of the internal combustion (IC) engine process is the most effective tool for design, performance evaluation and analysis. Modeling and simulation studies become critical while adopting new fuels with existing engine designs due to different thermo-physical properties<sup>1</sup> of the new fuel. Modeling and simulation studies also provide information about various interacting phenomena difficult to obtain from experimental investigations.<sup>2,3</sup>

Mathematical models range from simple zero-dimensional (0D) or thermodynamic models to exhaustive multi-dimensional (MD)<sup>3</sup> models. While 0D models require a predefined mass burn rate

defined empirically,<sup>3</sup> MD models evolve heat release profiles based on a phenomenological approach and empirical correlations apart from fundamental principles.<sup>4,5</sup> Zero D models offer the distinct advantage of superior and unmatched accuracy for performance evaluation and analysis<sup>6</sup> since predictions are based on empirical results obtained from basic experimental

Center for Sustainable Technologies, Indian Institute of Science, Bangalore, India

### Corresponding author:

Anand M Shivapuji, Center for Sustainable Technologies, Indian Institute of Science, Bangalore 560012, India.  
Email: anandms@cgpl.iisc.ernet.in

results. Zero D models permit parametric investigation with a fair degree of accuracy over a range of operating conditions where the empirical coefficients are determined.<sup>7</sup>

On the utility of the 0D models, the literature reveals successful use of 0D models for such wide applications as residual gas mass fraction measurement,<sup>8</sup> knock prediction<sup>9</sup> and full cycle simulations.<sup>10</sup> The recent literature also suggests significant emphasis at both industrial and academic levels on improving the prediction capabilities of zero D models.<sup>11</sup> The 0D models are emerging as viable alternatives and a critical tool for investigating and validating various strategies for optimizing the in-cylinder combustion process<sup>12,13</sup> with significant efforts being directed at full computational fluid dynamics derived 0D models considering the rapid simulation capabilities of such models.<sup>14</sup>

Bio-derived fuels are being explored towards meeting the energy needs for both heat and power, particularly as a mitigation option in the present scenario to address climate change issues. Research towards establishing the necessary tools for performance prediction and evaluation is important in the renewable energy sector. The focus of the current work is to analyse the combustion phasing of a spark ignited (SI) gas engine fuelled with producer gas (PG), generated from the thermo-chemical conversion of biomass. Producer gas has a typical composition (by volume) of 18–20% each of H<sub>2</sub> and CO, 2% CH<sub>4</sub>, 12% CO<sub>2</sub> and balance N<sub>2</sub>.<sup>15</sup> Thermo-physical properties like the laminar flame speed  $S_L$  (velocity of the unburned gases through and normal to the flame surface),<sup>16,17</sup> the adiabatic flame temperature (AFT) (peak attained by the products of combustion without heat loss from the system),<sup>17,18</sup> the lower calorific value (LCV) (heat of combustion with un-condensed moisture)<sup>18,19</sup> and product to reactant mole ratio for PG are different from conventional hydrocarbon fuels requiring a detailed analysis of the combustion phasing. Table I compares the properties of PG with some conventional fuels. It can be observed that though the LCV of the fuel is about a tenth of that of natural gas (NG), the LCV of the stoichiometric PG–air mixture is lower only by about 25% as compared to NG–air stoichiometric mixture. This is attributed to

the vastly different air-fuel (A/F) ratio for PG compared to NG. Another important property having significant difference is the stoichiometric laminar flame speed. PG flame speed at 0.50 m/s is over 40% faster than NG stoichiometric flame speed at 0.35 m/s.

Analysis of combustion of mixture containing H<sub>2</sub> is important considering that H<sub>2</sub> is seen to influence the flame propagation beyond the chemical kinetics realm. While H<sub>2</sub> enhances the flame speed due to a global increase in the reactivity,<sup>20–22</sup> it is also seen to promote structural instability and hence cellularity.<sup>23,24</sup> Higher cellularity promotes flame breakup into smaller cells causing an increase in the effective flame front area<sup>25,26</sup> and hence turbulent flame propagation speed. The presence of CO in nearly the same proportion as H<sub>2</sub> by volume makes the analysis that much more important since CO is seen to decrease thermal and diffusive instabilities as against H<sub>2</sub> which promotes the same. Since the thermo-physical properties of PG are different from conventional fuels and with H<sub>2</sub> and CO have counteracting influences on the flame stability and propagation, the heat release pattern and hence the combustion phasing in an engine is expected to be different. This makes the analysis of combustion phasing and hence the fixing of specific Wiebe coefficients critical.

Analysis of combustion phasing is possible by using the engine heat release profile.<sup>3</sup> The analysis provides information regarding the extent of similarity or difference between PG and conventional fuel(s) for which the engine is designed. Combustion phasing is represented in terms of an exponential curve fit by determining the shape and efficiency; Wiebe parameters for a heat release profile.<sup>3,27</sup> The Wiebe parameters are used in a Wiebe function, which describes the mass burn and hence heat release fraction in the engine. While Wiebe parameters for conventional fuels are established and optimized, estimation of Wiebe parameters for PG is justified considering that the heat release pattern for PG is expected to differ from that for conventional fuels. Using the values defined for other fuels could lead to significant deviation in the simulation.<sup>3,7</sup>

Literature survey indicates very limited fundamental work on producer gas engines in general. A significant portion of the available literature focuses exclusively on the performance analysis of producer gas based engines<sup>28–31</sup> and very limited work is reported on the in-cylinder investigations and modeling.<sup>2,32,33</sup> No work pertaining to the impact of fuel properties on the heat release pattern has been reported.

The current work also assumes significance because, though exhaustive literature is available on the use of the Wiebe function for internal combustion engine simulation,<sup>2,6,33–37</sup> hence highlighting its significance, critical review of the results indicate that even with the usage of different fuels with vastly

**Table I.** Thermo-physical properties of various fuels.

Fuel	Fuel LCV	A/F	Mixture LCV		$S_L$	AFT
	MJ/kg		MJ/kg	MJ/Nm <sup>3</sup>	m/s	K
	$\phi = 1$					
PG	05.00	1.35	2.12	2.53	0.50	1800
Gasoline	44.00	14.6	2.83	3.82	0.42	2100
NG (CH <sub>4</sub> )	50.20	17.2	2.76	3.40	0.35	2210
Butane (C <sub>4</sub> H <sub>10</sub> )	45.50	15.39	2.77	3.67	0.44	2250

LCV: lower calorific value; AFT: adiabatic flame temperature; A/F: air-fuel ratio; PG: producer gas; NG: Natural gas.

different thermo-physical properties, Wiebe parameters for conventional fuels are adopted for simulation.<sup>38,39</sup> Instances of the use of conventional Wiebe parameters for fuels with MBT ignition timing varying between 30° before top dead center (BTDC) and 4° BTDC (highlighting the drastic variations in the thermo-physical properties) are also found.<sup>40</sup>

The present research highlights the criticality of fuel-specific Wiebe coefficients by establishing the combustion phasing and Wiebe parameters for PG as a fuel. The established Wiebe parameters are subsequently used in a 0D simulation to predict performance parameters like the position and magnitude of the peak pressure and to evolve the pressure-crank angle profile. Simulation results from the model are compared with experimental results for different operating conditions. To generalize the modeling effort, the comparison is extended to different engine geometry and compression ratios (CR).

## Methodology

Experimental investigations involved acquiring in-cylinder pressure traces along with other engine parameters on a PG-fuelled 6-cylinder engine of Cummins India Limited (CIL) make (6B5.9) in both naturally aspirated (NA) and turbo-charged after-cooled (TA) mode for a fixed CR of 10.5. Experiments under both NA and TA modes of operation were carried out at maximum brake torque (MBT) conditions at stoichiometry. Pressure traces from a 3-cylinder engine of Kirloskar Oil Engines (KOE) make (RB33) at different CR's fuelled with PG at stoichiometry and MBT conditions available from a previous work<sup>41</sup> are also used in the analysis. Comparisons are made with fossil fuels like gasoline and NG. Using the first law, the pressure trace is converted to net heat release trace. The Wiebe parameters are obtained by means of least square curve fit and subsequently used in 0D simulation.

## Experimental setup

Experimental data from two engines with different specifications are used for the analysis. The engine designated *E1* (6B5.9) is a 50 kW<sub>e</sub> (rated capacity with NG as the fuel) 6-cylinder inline engine while the engine designated *E2* (RB33) is a 28 kW<sub>e</sub> (rated capacity with diesel as the fuel) 3-cylinder diesel engine converted to SI configuration to operate on PG. The engine specifications are as presented in Table 2. The conversion of the diesel engine into a SI engine was done by insertion of spark plugs in place of fuel injectors and adoption of a 3-cylinder distributor type battery-based ignition system.<sup>41</sup> Engine *E1* is operated in both NA and TA modes while *E2* operates only in NA mode.

The engine *E1* designed to operate on NG was modified to operate on producer gas using a specially

**Table 2.** Specifications of the engines used for the experiments.

Parameter	Engine <i>E1</i>	Engine <i>E2</i>
Make and model	Cummins, 6B5.9	Kirloskar, RB33
Engine type	In-line, 6 cylinder, 4-stroke	In-line, 3 cylinder, 4-stroke
Aspiration	Natural/ Turbocharged	Natural
Rated output	50 kW <sub>e</sub> on NG	28 kW <sub>e</sub> on diesel
Speed	1500 r/min	
Cooling type	Water cooled with radiator	
Bore × Stroke	102 × 120 mm	110 × 116 mm
Compression ratio	10.5 : 1	17 : 1 (base)
Piston type	Cylindrical bowl	Hemispherical bowl
Firing order	1-5-3-6-2-4	1-2-3

designed carburettor<sup>31</sup> operating in conjunction with a zero pressure regulator to accommodate the high mixture flow rate. The experimental pressure traces from engine *E1* are used for establishing the Wiebe coefficients and the simulation results using these coefficients are subsequently used to compare with the experimental results of both engines *E1* and *E2*.

The in-cylinder pressure is measured using an AVL make spark plug adapted uncooled piezo-electric (gallium orthophosphate) pressure sensor (GH13Z) at an acquisition frequency of 9 kHz. Differential pressure data to absolute pressure conversion is by using the manifold pressure sensor with a reference pressure supplement. The absolute pressure measurement across the compressor and turbine of the turbo-charger is done by using a line pressure sensor with an absolute pressure supplement. Measured data from the connected instruments is acquired by using an 8-channel data acquisition module (AVL IndiModul) and real time processing and display by means of a graphical user interface (AVL IndiCom). Detailed specifications of the instrumentation are presented in Table 3. Air and gas flow rates are measured using venturimeters and temperature is measured using K-type thermocouples. Gas composition is measured using SICK MAIHAK make online gas analyzer while the exhaust gas analysis was done using a QUINTOX make flue gas analyzer.

## Model formulation

### First law analysis

A 0D model based on the first law<sup>3,42</sup> is developed to predict the evolution of cylinder pressure during the cycle. The gas exchange process is modelled along the filling and emptying technique (FET)<sup>43</sup> and mass flow through the various volumes is modelled using the 1D isentropic flow equation for compressible flow.

The literature reports the filling and emptying process to be between isothermal and adiabatic<sup>44,45</sup> and the pressure fluctuations in the elements are modelled using the first law for an open system as in equation (1) where  $P$ ,  $V$  and  $Q$  represent the pressure, volume and heat transferred with  $\theta$  representing the crank angle. The symbols  $\gamma$ ,  $m$  and  $c$  represent the polytropic index, mass and sound velocity respectively. The subscripts 'i' and 'e' represent the inlet and exit conditions respectively.

$$\frac{dP}{d\theta} = \frac{(\gamma - 1)dQ}{V} - \gamma \frac{P dV}{V} + \frac{(\gamma - 1)}{V} \left[ \frac{c_i^2}{(\gamma_i - 1)} \frac{dm_i}{d\theta} - \frac{c_e^2}{(\gamma_e - 1)} \frac{dm_e}{d\theta} \right] \quad (1)$$

**Coefficient of discharge for flow through valves**

The discharge coefficient,  $C_d$  for the intake and exhaust valves is evaluated as a function of the

valve lift  $l_v$  to valve diameter  $d_v$  ratio as discussed in Heywood<sup>3</sup> and Ferguson and Kirkpatrick<sup>42</sup> and described in equation (2). The discharge coefficient results as indicated in Figure 1 are consistent with values reported by Annand and Roe<sup>46</sup> for valve geometry similar to that in the current investigation.

$$C_d = 107.78 \left[ \frac{l_v}{d_v} \right]^4 - 77.204 \left[ \frac{l_v}{d_v} \right]^3 + 14.1 \left[ \frac{l_v}{d_v} \right]^2 - 1.01 \left[ \frac{l_v}{d_v} \right] + 0.6687 \quad (2)$$

Cylinder pressure is evaluated from equation (1) during the gas exchange processes by retaining the mass flow terms, while for the compression-expansion process with intake and exhaust valves closed, the mass flow terms from the equation are eliminated by neglecting leakage.

**Wiebe function and coefficients**

The energy released in the engine cylinder due to combustion is modelled using the Wiebe function developed by I. I. Wiebe<sup>47</sup> based on the law of normal distribution of a continuous random variable.<sup>48</sup> The Wiebe function, used to predict the mass burn fraction in an engine is of the form as in equation (3).

$$\frac{Q_{chem}(\theta)}{Q_{chem-total}} = 1 - \exp \left[ -1 \left( \frac{\theta - \theta_{soc}}{\Delta\theta} \right)^{m+1} \right] \quad (3)$$

The constant  $m$  is the shape factor, while  $a$  is the efficiency factor indicative of the fuel conversion efficiency  $\eta_c$  as in equation (4). The subscripts 'soc' and 'doc' indicate the start and duration of combustion, respectively.

**Table 3.** Specifications of the engine instrumentation.

Description	Model	Specifications
Cylinder pressure	GHI3Z-24	Measuring range 0–250 bar Load cycles 10 <sup>8</sup>
Line pressure	QC34C	Measuring range 0–250 bar Load cycles 10 <sup>8</sup>
Angle encoder	365C	Speed range 20,000 r/min Resolution 0.1° CA
Indicating system	IndiModul	Channels 8 Resolution 14 bit Sampling rate 800 kHz/ch Internal memory 64 MB

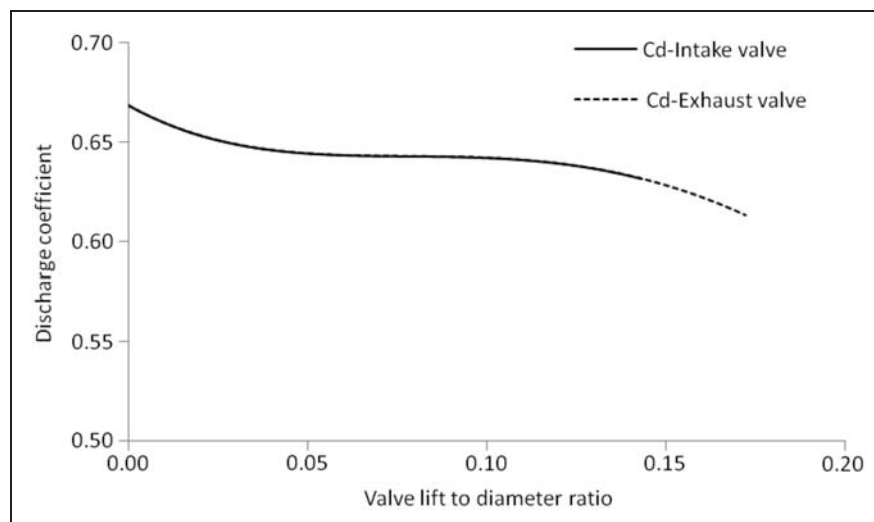


**Figure 1.** Variation of the discharge coefficient as a function of valve lift-to-diameter ratio.

$$\eta_c = \frac{Q_{chem}(\theta)}{Q_{chem-total}} = 1 - e^{-a} \quad (4)$$

An efficiency factor of 5 and a shape factor of 2 have been arrived at for typical hydrocarbon fuels.<sup>3,47,49</sup> On the versatility of the Wiebe function in capturing heat release profiles, Figure 2 shows the impact of combustion duration and shape factor on the heat release profile as evaluated from equation (3).

The heat release profiles, designated as fraction of heat release (FoHR) are plotted for three different shape factors of 1, 2 and 3 for two combustion durations of 40° and 80°, respectively. The choice of shape factor(s) has been made to assess the Wiebe function response on either side of the conventional choice of 2. The peak (fractional) heat release rate (PHRF) is plotted at 10° intervals from 40° to 80° duration for the three shape factors. As evident from Figure 2, the shape factor governs the peak heat release rate and its position. An increase in the shape factor displaces the position of peak heat release rate towards the end of combustion while the shape of the profile changes from being predominantly convex to concave as observed from the origin. This behavior is independent of the combustion duration and is hence used as a critical parameter to match the desired profile.

The literature<sup>50</sup> indicates choice of efficiency factors as high as 6.9 and 10 in an effort to match the Wiebe heat release profile with the experimentally observed profiles.<sup>51</sup> Choice of efficiency factor as high as 10 is rather surprising considering that the fuel conversion efficiency attains a value of 99.32% at  $a=5$  and changes to 99.99% for  $a=10$ . The fuel conversion efficiency in a typical SI engine seldom crosses 98% even under lean conditions.<sup>3</sup> Tuning of  $a$  to match the heat release profile thereby seems unrealistic and is thermodynamically untenable.

In the present work, the efficiency factor  $a$  is estimated on the basis of exhaust emissions measurement reflecting the combustion efficiency, giving a fair degree of legitimacy for the choice, while the shape factor is tuned to reproduce the experimental heat release profile. The choice of  $m$  and the combustion duration are governed by the requirement of the heat release profile to reproduce the primary combustion descriptors available from the experimental results within acceptable limits of deviation. The importance of combustion phasing and its impact on the maximum power output as well as cycle to cycle variations have been brought out by Pipitone<sup>52</sup> for gasoline and extended to PG by the current authors.

### Heat transfer at the engine wall

The engine wall heat transfer is calculated using equation (5), which represents the heat flux on the gas side. The radiation component of the heat transfer is neglected since it constitutes less than 5% for a typical SI engine.<sup>3,42,53</sup>

$$\dot{q} = h_{c,g}(\bar{T}_g - T_{w,g}) \quad (5)$$

The heat transfer process is considered as quasi-steady<sup>3,54</sup> and is justified, as the variation in actual heat transfer is a very small fraction of the total heat flux when the heat transfer coefficient fluctuates. Various models have been proposed by Annand,<sup>54</sup> Woschni,<sup>55</sup> Hohenberg<sup>56</sup> and other researchers for quantifying the gas side convective heat transfer coefficient  $h_{c,g}$  (for mean gas temperature  $\bar{T}_g$  and wall temperature  $T_{w,g}$ ). All the correlations have a general form with the Nusselt number ( $Nu$ ) being expressed as a function of Reynolds number ( $Re$ ) and Prandtl number ( $Pr$ ). The correlation proposed by Annand as in equation (6) is used in the present analysis.

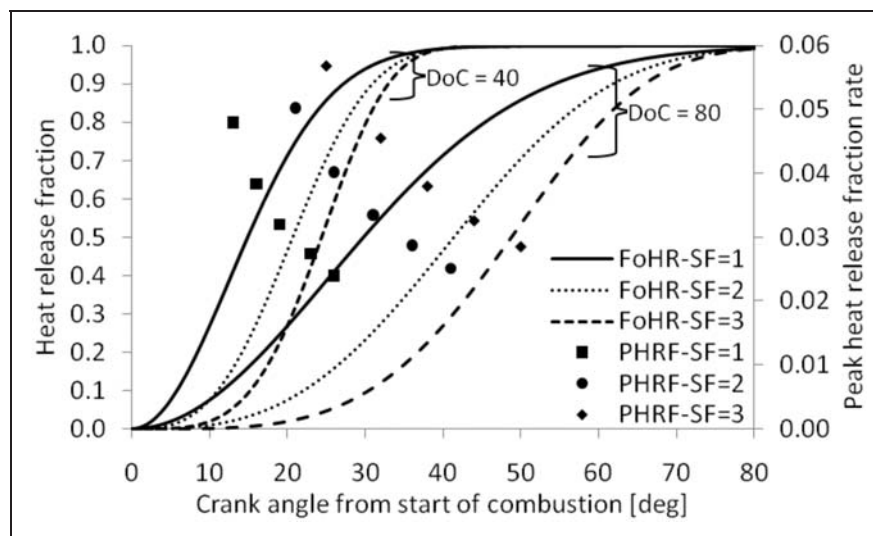


**Figure 2.** Effect of combustion duration on the heat release profile and the peak heat release rate. FoHR: fraction of heat release; PHRF: peak (fractional) heat release rate.

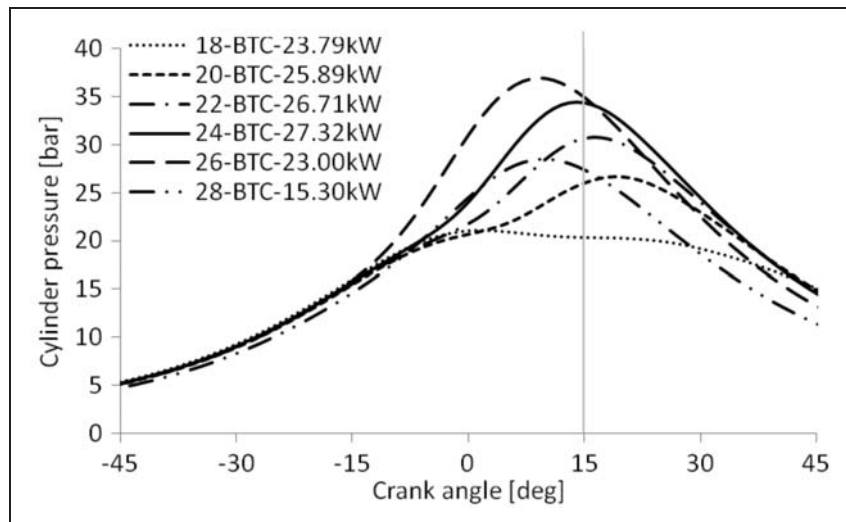


**Figure 3.** Pressure-crank angle trace for NA operation of E1 at various ignition angles. BTC: before top center; NA: naturally aspirated.

In equation (6) the values of  $d$  and  $b$  depend on flow properties within the engine cylinder while  $k$  and  $B$  are the thermal conductivity of the gases and linear dimension.  $\bar{S}_p$ ,  $\mu$  and  $\rho$  indicate the mean piston speed, dynamic viscosity and density, respectively.

$$h_{c,g}(\theta) = d \frac{k}{B} \left( \frac{\rho \bar{S}_p B}{\mu} \right)^b \quad (6)$$

## Experimental results

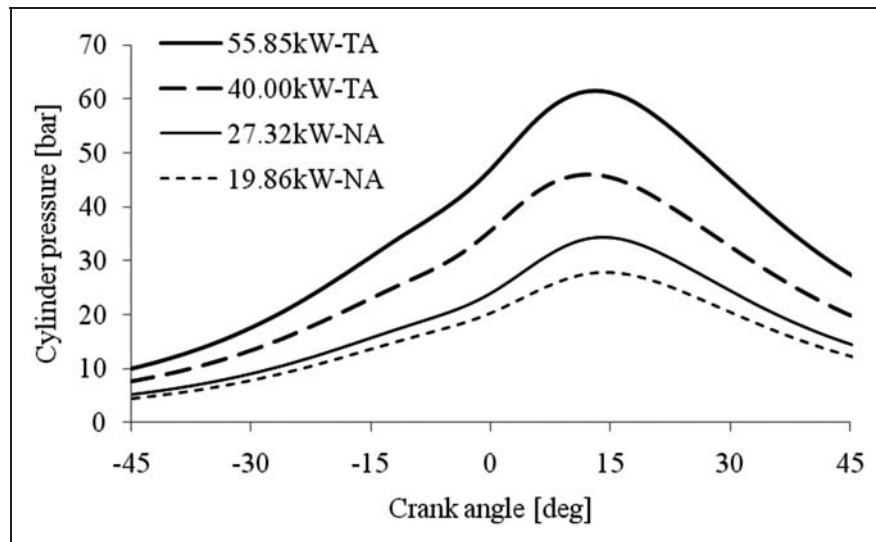
This section presents the results from the experiments conducted on engine E1. The pressure trace(s) for E1 under NA and TA modes and E2 under NA mode are ensemble averages of 250 and 30 consecutive cycles, respectively. The spark sweep test was used to determine the MBT timing and further examined using the combustion descriptor(s) at MBT conditions for E1 under NA operation. For TA operation, the position of peak pressure was adopted for establishing the MBT timing. Figure 3 presents the results from the spark sweep test under NA conditions for the engine E1. The MBT timing is found to be 24° BTDC.

From the pressure trace the position of peak pressure is found to be in the range of 14°–16° after top dead center (ATDC) at 24° BTDC ignition confirming the outcome of the spark sweep test. For the TA mode of operation, the spark was timed to allow the position of peak pressure to be in the range of 14°–16° ATDC for positioning the engine at MBT timing. The position of peak pressure was observed to be in the desired range for 22° BTDC ignition setting indicating the same as MBT timing. A full range load test was carried out for both NA and TA mode under respective MBT ignition timings. Figure 4 presents the pressure crank angle trace for NA and TA modes of operation where, for brevity only two loads representing 100% and around 70% at MBT conditions for

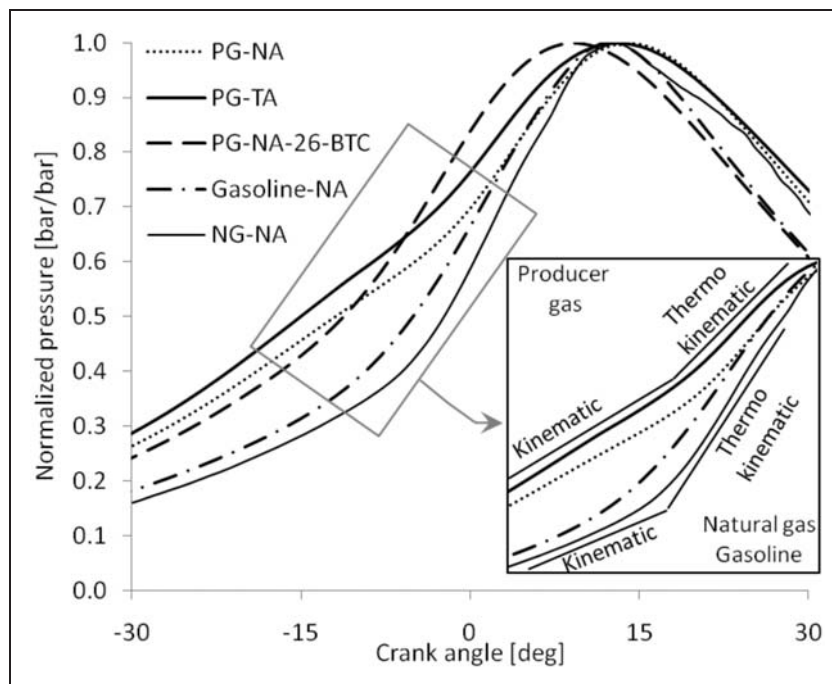
both NA and TA operations are reported. The engine delivered a peak load of 55.85 kWe under turbocharged conditions amounting to an increase of 104% over NA peak load of 27.3 kWe.

Figure 5 compares the peak load normalized pressure trace at MBT for PG operation under NA and TA modes of operation with the pressure trace using NG as the fuel on the same engine and a general stoichiometric gasoline profile. The pressure crank angle trace for PG when compared with NG and gasoline traces indicates difference in pressure profile development especially in the 15° BTDC to 5° ATDC range. This region is magnified and presented separately as an inset in Figure 5. Approximate slope lines indicative of the kinematic (compression only) and thermokinematic (compression and heat release) contributions to the pressure rise are indicated for PG and NG/Gasoline operation separately. Change in the slope during the transition from kinematic to thermokinematic pressure rise indicates a very small value (equivalent of 12°) for PG as compared to (43°) NG/Gasoline operation. In order to understand the differences in pressure profile development, further investigation into the variation of the rate of pressure rise with crank angle was carried out as subtle differences, if any, would be evident in the pressure rise rate (PRR) against crank angle profile. The rate of pressure rise is another combustion descriptor used for the analysis of combustion phasing.<sup>52</sup> The PRR profile for the considered cases is plotted in Figure 6.

The PRR profile(s) clearly identifies the subtle differences between PG and NG/gasoline operation which is not evident in the pressure crank angle trace. For a typical engine, under motoring conditions the peak pressure is positioned in the immediate vicinity of the TDC while the PRR peaks around 18° BTDC. The PRR starts to decrease beyond 18° BTDC due to the decelerating piston reaching zero



**Figure 4.** Variation of cylinder pressure with crank angle for EI testing in NA and TA modes. NA: naturally aspirated; TA: turbocharged after-cooled.



**Figure 5.** Variation of normalized cylinder pressure for gasoline, NG and PG (on engine EI) under MBT conditions. NG: natural gas; PG: producer gas; MBT: maximum brake torque; NA: naturally aspirated; TA: turbocharged after-cooled; BTC: before top center.

velocity at the TDC; where the piston reverses the direction of movement. For a firing cycle using fuels like NG and gasoline, under MBT operation the in-cylinder heat release rate would attain a sufficient thermodynamic condition around  $18^\circ$  BTDC so as to offset the kinematics-driven reduction in the PRR such that both the pressure and the PRR continue to increase. The PRR profile in the closed part of the cycle in-cylinder process would be unimodal as evident from Figure 6. The difference between PG and NG/gasoline pressure profile arises from the fact that

the PRR profile for PG operation suggests bimodal behavior as against the unimodal response for NG and gasoline.

The bimodal pattern of the PRR profile for PG-fuelled operation with local maxima before the TDC suggests a possible delay in the initial flame kernel development. This deferment of the heat release in the initial stages causes the PRR to drop from the local maximum with the crank angle. However, as the piston approaches TDC, the PRR increases due to the corresponding increase in the heat release. The

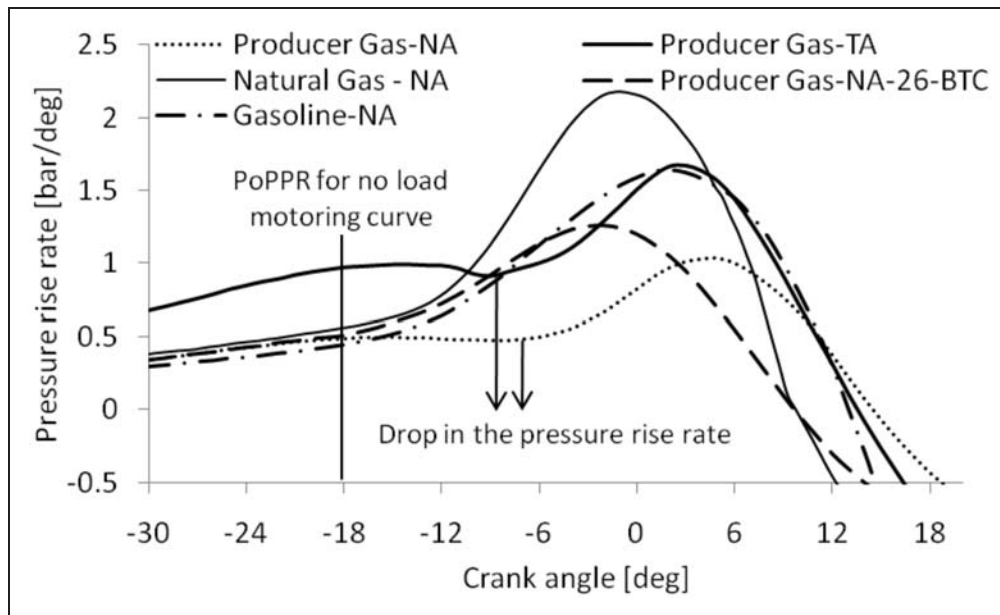


**Figure 6.** Variation of pressure rise rate for gasoline, NG and PG (on engine *E1*) under MBT conditions. NG: natural gas; PG: producer gas; MBT: maximum brake torque; NA: naturally aspirated; TA: turbocharged after-cooled; BTC: before top center.

heat release driven pressure rise dominates over the kinematics-driven pressure drop. Another aspect is that even though both NA and TA modes of operation indicate a bimodal profile, the drop in the PRR from the first local maximum to the next minimum is much steeper for TA operation (0.079 bar/deg) than for NA operation (0.024 bar/deg). The difference arises due to the TA MBT timing being 2° retarded compared to NA MBT timing. In the TA mode, the significantly severe in-cylinder thermodynamic conditions as compared to the NA mode, does not seem to have any significant impact on the initial flame kernel development period. The difference in the pressure profiles for the same engine kinematics suggests the influence of the fuel thermo-physical properties on the engine operation play an important role.

In order to address the difference in the engine response in the case of PG operation, the properties of PG are critically reviewed. The presence of nearly 20% volume fraction of  $H_2$  in the fuel and its influence on the overall laminar flame speed<sup>57</sup> is addressed. Wang et al.<sup>58</sup> using NG– $H_2$  mixtures in a constant volume bomb experiments provide photographic evidence towards establishing the initial flame kernel development period being independent of  $H_2$  concentration. However, once the flame kernel is fully formed, the flame propagation stage is strongly influenced by the presence of  $H_2$ , with higher hydrogen fractions causing faster flame propagation. The pressure profile of *E1* with PG can be explained based on the experimental results on the presence of  $H_2$  in the fuel by Wang et al.

The bimodal nature of the PRR profile while positioning the peak pressure around 15 deg ATDC while indicating a delay in the flame kernel development

also suggests rapid flame propagation for PG as compared to NG/Gasoline. The typical response for PG operation is associated with the presence of  $H_2$  in PG. With the flame kernel development period being independent of the concentration of  $H_2$  as indicated by Wang et al.,<sup>58</sup> the retarded ignition setting for PG-fuelled operation leads to the kinematics-driven drop in the PRR not being compensated by the combustion-driven heat release. However, once the flame kernel reaches a certain critical diameter or mass burn fraction, the flame propagation speeds up due to global increase in the reaction rates and the enhanced cellularity<sup>25,26</sup> associated with  $H_2$  containing flames. This increase in the flame speed causes the cylinder peak pressure to be positioned at around 15° ATDC.

### Heat release profile

The heat release profile is evaluated for the region between 60° BTDC and 90° ATDC on the basis of equation (1). The polytropic index for compression and expansion processes is evaluated from the slope of the best straight line fit on the  $\log(V)$  with  $\log(P)$  plot.<sup>3</sup> Figure 7 shows a typical  $\log(V) - \log(P)$  graph for the wide open throttle (WOT) operation for the engine *E1*.

Figure 8 presents the heat release pattern for engine *E1* at various ignition angles with a typical gasoline heat release curve for comparison. The general observation is that the heat release pattern for PG differs significantly from the gasoline heat release profile. Even though the PG heat release trace approaches the gasoline heat release trace as the MBT condition is approached, differences are evident especially in the 50% to 100% heat release range. Figure 9 compares

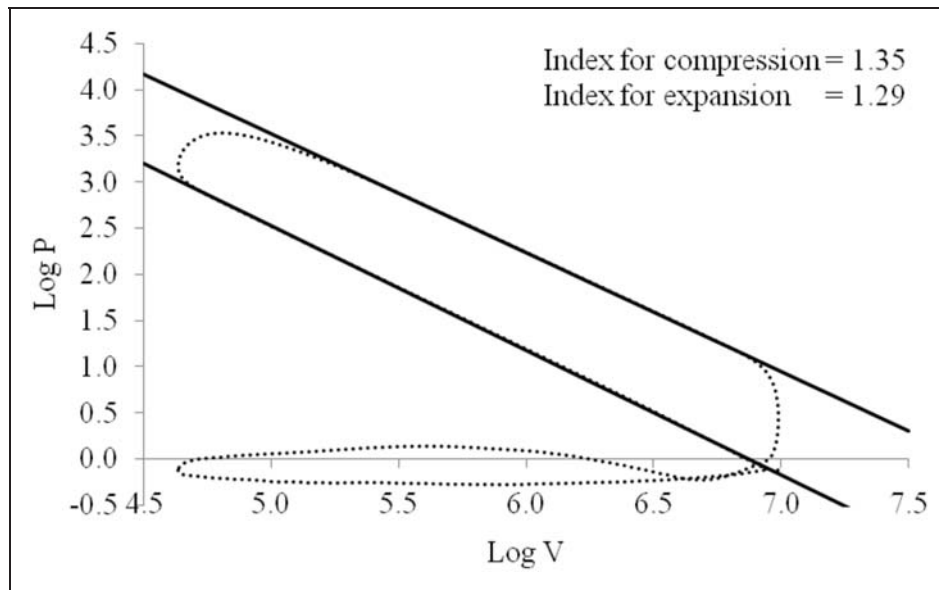


**Figure 7.**  $\log(V)$  vs  $\log(P)$  plot for EI at MBT ignition and WOT condition. MBT: maximum brake torque; WOT: wide open throttle.

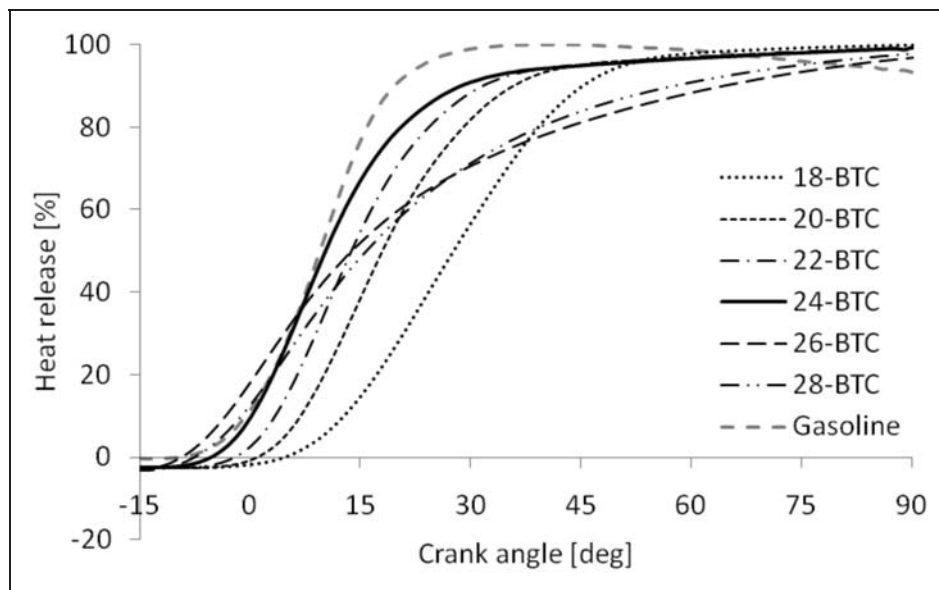


**Figure 8.** Heat release profiles for EI at various ignition angles compared with gasoline profile. BTC: before top center.

the PG heat release trace for 100%, 70% and 50% of peak load for NA and TA modes with the gasoline-fuelled engine heat release trace. The peak load combustion durations in terms of degrees of crank angle for gasoline and NA/TA mode of operation are included as an inset for the first and second half of the combustion. The difference in combustion duration in the first and second half is evident from the data present in the inset. PG combustion tends to be sluggish in the second half, leading to an overall increase in the combustion duration. Among the PG profiles, the heat release profile for the advanced ignition settings differs significantly compared to MBT

and retarded settings. At advanced ignition settings, the heat release profile deviates from the typical *S* profile, characteristic of SI operation. The rather slow heat release and corresponding extended combustion duration are manifested in the form of drastic reduction in the supported load. This is evident from the data presented in the inset in Figure 3, which indicates a load drop of 16% and 44% for 2° and 4° advanced ignition from MBT compared to 2% and 13% drop for corresponding retarded ignition settings.

Further comparison between gasoline and PG suggest that, the first half combustion duration being the same for gasoline and PG operation (both NA and

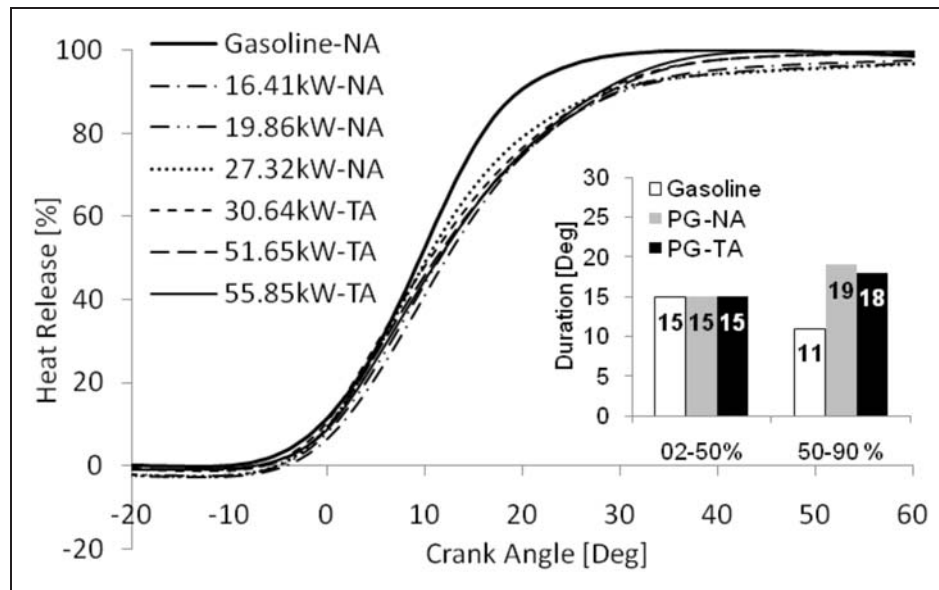


**Figure 9.** Comparison of normalized heat release profiles and combustion duration (inset) for PG on engine EI with gasoline. NA: naturally aspirated; TA: turbocharged after-cooled; PG: producer gas.

TA modes) confirms the earlier discussion on the bimodal nature of the PRR trend where it was mentioned that  $H_2$  has insignificant influence on the initial flame kernel development period. The 50–90% region response is argued to be influenced by the thermo-physical properties of PG. Before reasoning the causes for such a behavior, it is critical to highlight the fact that under MBT settings, at about 15° ATDC, the flame would approach the farthest wall of the cylinder and the cylinder pressure would peak.<sup>3</sup> However, at this stage, the entire mixture would not have been consumed and the mass burn fraction would still be around 70%.<sup>3</sup> Essentially, the last 30% of the mixture would be concentrated near the cylinder walls and within the unburned pockets of the turbulent flame bush.

The presence of nearly 20%  $H_2$  in the gas enhances the overall flame speed and subsequently the position of peak pressure is recorded in the vicinity of 15° ATDC for MBT conditions. However, when it comes to the combustion of the remaining nearly 30% of the mixture, two critical adverse impacts due to the presence of  $H_2$  need attention.  $H_2$  enhances the thermal diffusivity of PG (0.61 cm/s for  $H_2$  against 0.05 cm/s and 0.16 cm/s for gasoline and  $CH_4$  respectively)<sup>59</sup> while reducing the flame quenching distance (0.2 cm for gasoline and  $CH_4$  against 0.06 cm for  $H_2$ ). High flame speed and high thermal diffusivity leads to increased heat transfer to the cylinder wall due to enhanced convection from the burning gases while lower quenching distance reduces the thermal boundary layer thickness, again enhancing the heat transfer to the cylinder wall. Enhanced heat loss to the coolant is manifested in the engine cooling load. Heywood<sup>3</sup> reports the cooling load to be around 25% of the input energy for SI engines while cooling loads in

the present PG operation have been in excess of 30% for both NA and TA modes of operation as indicated in Figure 10. Increased cooling losses for PG operation have also been reported by Rao.<sup>41</sup> The complete parametric investigation of the engine in NA mode of operation on the basis of which the heat balance sheet is drawn up is presented in a different work<sup>60</sup> by the present authors.

The influence of  $H_2$  on enhanced thermal diffusivity and quenching distance causing increased heat loss to the coolant has been explicitly confirmed by Ma et al.<sup>61</sup> in a work on varying  $H_2$ -CNG blends. Ma et al. have shown that the cooling loss for 100% CNG operation to be less than 15% of the input energy and increased to around 20% for 50% CNG- $H_2$  blend. Similar observations have been made by Shudo et al.<sup>62</sup> Thus, the enhancement of the combustion duration in the second half is attributed to the cooling of the mixture near the wall leading to flame de-speeding and increased combustion duration. The near wall mixture cooling assumes significance considering the fact that the thermal boundary near the wall has 30% to 40% of the total cylinder mass,<sup>63</sup> contributing significantly to the total combustion duration. Further, the absence of knock at advanced ignition conditions as evident from both pressure crank angle and heat release trace(s) can also be attributed to enhanced cooling of the mixture near the cylinder boundary. Considering the significant influence of the presence of  $H_2$  in PG, it is important that further additional investigations on the combustion within the engine cylinder should be addressed.

The qualitative explanation of the identified behavior of enhanced combustion duration in the second half of the heat release cycle and absence of any

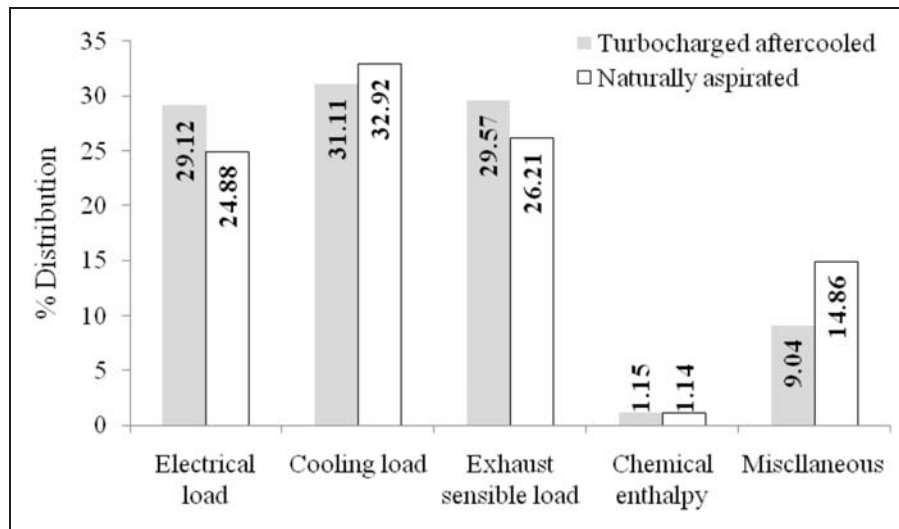


**Figure 10.** Energy balance for NA and TA mode of peak load operation on engine E1. NA: naturally aspirated; TA: turbocharged after-cooled.

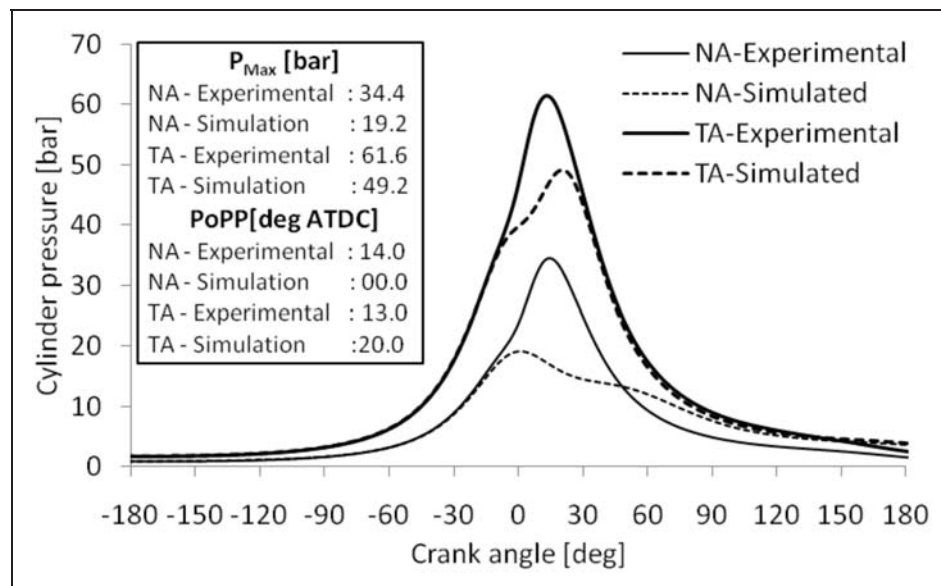


**Figure 11.** Comparing 0D simulation with experimental pressure trace using standard Wiebe coefficients. NA: naturally aspirated; TA: turbocharged after-cooled.

abnormal combustion requires further investigations to quantify these parameters, not in the scope of the present article.

The foregoing discussions pertaining to both pressure and heat release pattern highlight the criticality of the current work aimed at identifying fuel-specific Wiebe parameters for producer gas.

### Estimation of Wiebe curve fit coefficients

On the basis of the results presented in the previous sections, it is evident that significant differences exist between PG and gasoline with regard to combustion phasing. Figure 11 presents the comparison of experimental and modeling results from the 0D model using

conventional Wiebe parameters of  $m=2$  and  $a=5$ .<sup>3,42</sup> It is obvious that significant deviations exist between the experimental and modeling results. The data presented in the inset quantifies the differences for the peak cylinder pressure and its position. In the case of TA operation, the peak cylinder pressure is under-predicted by about 20% while the NA mode indicates retarded ignition. These results coupled with the previous discussions on the heat release pattern sufficiently justify the need for fuel-specific Wiebe coefficients for PG.

For estimating the Wiebe efficiency factor  $a$ , detailed measurements on the engine exhaust composition and temperature are used. Analysis of dry exhaust composition at higher loads has shown the

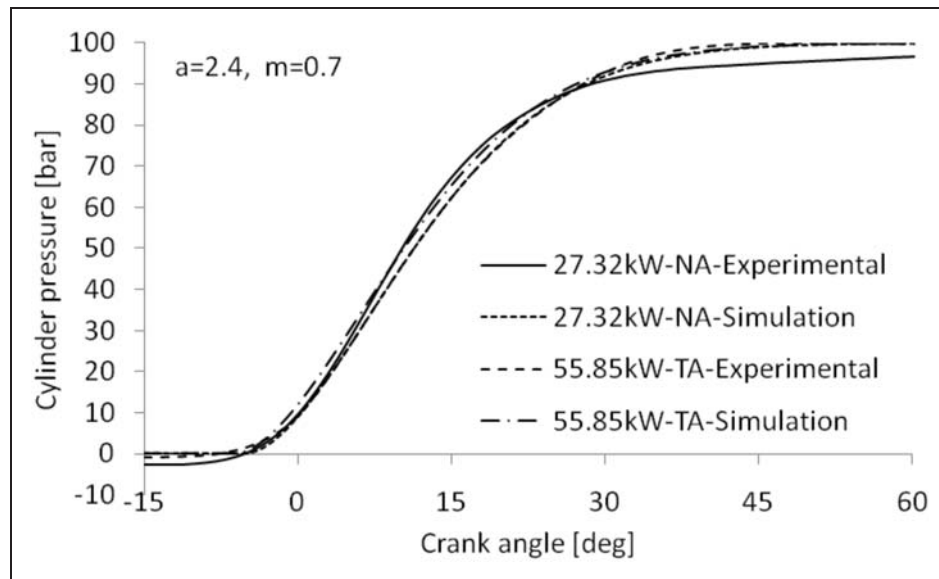


**Figure 12.** Comparison of experimental and Wiebe simulation results under NA and TA conditions for the engine E1. NA: naturally aspirated; TA: turbocharged after-cooled.

presence of CO in the range of 0.75% to 1.3% on mass basis and the exhaust gas temperature in the range of  $830 \pm 10$  K. This data is used in equation (7)<sup>3</sup> for estimating the combustion inefficiencies.

$$1 - \eta_c = \frac{\sum_i X_i Q_{HV_i}}{F/A Q_{HV_f}} \quad (7)$$

Measurements on PG composition and subsequent analysis indicate the stoichiometric fuel air ratio ( $F/A$ ) to be  $0.75 \pm 0.02$  and the LCV  $Q_{HV_f}$  to be  $4.1 \pm 0.05$  MJ/kg. Considering LCV  $Q_{HV_i}$  and mass fraction  $X_i$  for CO as 10.01 MJ/kg and 0.013, respectively, the conversion inefficiency amounts to about 5%. The high exhaust gas temperatures for PG operation (by 70–80 K) could be related to the in-cylinder combustion process and indicate late burning with reduced contribution to the work transfer. The sensible heat corresponding to 75 K evaluates to another 5% of the input energy. The above two factors amount to about 10% compared to a typical fossil fuel combustion where the inefficiencies are in the range of 1–2% of the input fuel energy.<sup>3</sup> On the basis of 90% fuel conversion efficiency, the value of efficiency factor is found to be 2.4 from equation (4). The shape factor for various conditions for PG operation was determined from the least square method and is estimated at 0.7 for PG for both NA and TA modes of operation. The 2% to 90% range is considered for the curve fit which is reasonable since the start and end of combustion cannot be exactly quantified.<sup>3,51,64</sup> Figure 12 presents the comparison between experimental and Wiebe simulation heat release profiles and as is evident, PG-specific coefficients based simulation provides close match to experimental results.

## Results and discussions

The PG-specific Wiebe coefficients are used in the 0D model and the pressure-crank angle traces compared with the experimental results. The CA is represented from  $-180^\circ$  BTDC to  $180^\circ$  ATDC in comparing the experimental and simulation results. This range is used to compare the gas exchange, compression, heat release and expansion processes in the engine cycle.

Figures 13 and 14 present the comparison between the experimental and the model predictions for the PG-fuelled engine at three different loads (representing  $\sim 20\%$ ,  $\sim 50\%$  and  $100\%$  loading) under NA and TA modes of operation for the engine E1. A near complete match of the experimental and the model predictions for both NA and TA modes of operations is observed. No quantifiable differences are observed in the magnitude of peak pressure.

Having established the versatility of PG-specific Wiebe parameters for engine E1, the analysis is extended to a different engine configuration and different compression ratios. Model predictions are carried out for engine E2 at two different compression ratios of 11.5 and 13.5. Figure 15 presents the comparison between the experimental and modeling pressure traces for the engine E2. A very close match is obtained for CR 11.5 with the peak pressure matching to the first decimal while the position of peak pressure differs only by a degree. However, in the case of CR 13.5, the magnitude of peak pressure is slightly low and the position gets slightly advanced from the TDC. It is assessed that high CR would entail higher in-cylinder temperatures (about 50 K higher for CR 13.5 than for CR 11.5 for motoring conditions based on polytropic assessment) and correspondingly

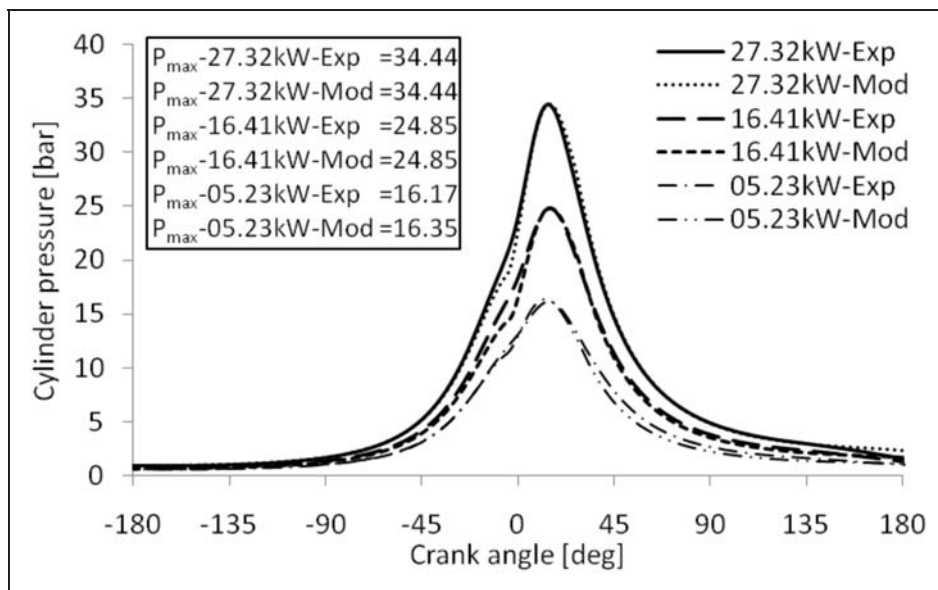


**Figure 13.** Comparison of experimental and simulated pressure traces at various loads for NA operation. NA: naturally aspirated.

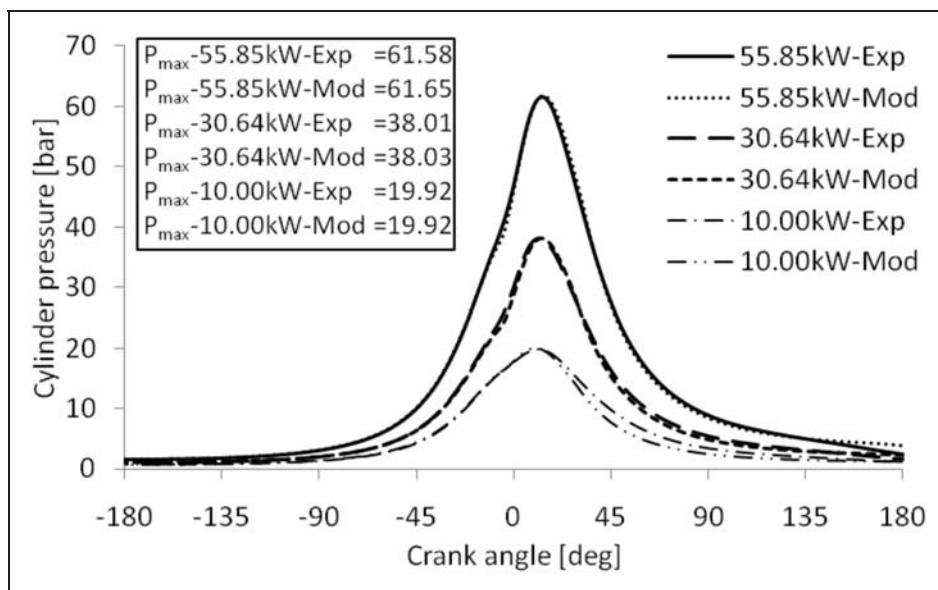


**Figure 14.** Comparison of experimental and simulated pressure traces at various loads for TA operation. TA: turbocharged after-cooled.

influence the flame speed, resulting in reduced combustion duration and altered combustion phasing. From the figure it can be concluded that advancing the end of combustion angle would shift the pressure profile to match the experimental trace and accordingly, the end of combustion angle is reduced by about  $6^\circ$ . Using the advanced condition of combustion angle results in near complete reproduction of the experimental pressure trace implying higher burn rates at higher CR. The above result further strengthens the generality of the fuel-specific Wiebe coefficients wherein the same coefficients could be used

for a different geometry and CR while requiring the tuning of combustion duration. Tuning of the combustion duration is not only desirable and is consistent with the in-cylinder thermodynamics, but also a mandatory requirement even for physical operation of the engine to retain the original operating point with a change in the CR, which is managed by changing the ignition timing. The ignition timing is retarded with increasing CR (shorter combustion duration) and advanced with reducing CR (longer combustion duration) to phase the combustion to deliver maximum torque.

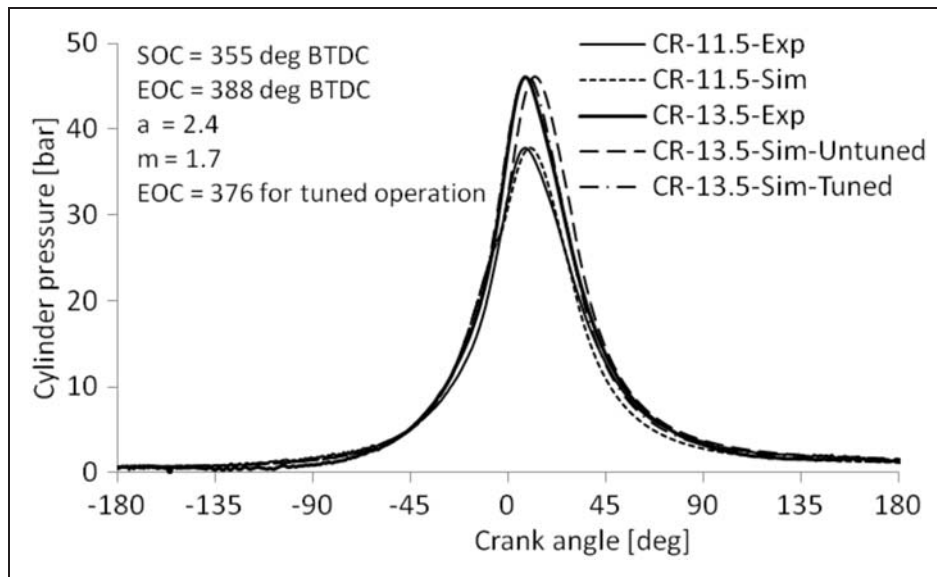


**Figure 15.** Comparison of experimental and simulated traces for E2 under WOT-MBT operation. WOT: wide open throttle; MBT: maximum brake torque; BTDC: before top center.

## Conclusions

The research work has shown evidence towards the need for change in the Wiebe coefficients using producer gas as a fuel whose thermo-physical properties are different from those of a fossil fuel. Experiments on a 6-cylinder engine fitted with a turbo-charger generated power of 55.9 kWe, an increase of around 104% over NA peak load of 27.3 kWe. MBT timing along with position of peak pressure has been used as the criterion for peak load condition for the experimental analysis. The presence of H<sub>2</sub> has been found to influence various phases of in-cylinder combustion. Presence of H<sub>2</sub> is seen to increase the overall burning rate but the impact on the initial flame kernel development period is negligible while owing to the high thermal diffusivity and lower quenching distance, heat loss from the gases to the cylinder walls is seen to increase.

The 0D model adopts the Wiebe function for the heat release and Annand's heat transfer correlation to predict the engine pressure traces. It has been shown that the use of producer gas needs change in the efficiency factor and the shape factor to match the experimental heat release profile. With  $a = 2.4$  and  $m = 0.7$ , the pressure traces for various operating conditions in naturally aspirated and turbo-charged conditions have been compared with the experimental results. Further, the model has been used to predict the pressure profile for a 3-cylinder engine configuration and the simulation results compare well with the experimental results.

## Funding

This work was supported by Ministry of New and Renewable Energy, Government of India, New Delhi.

## Acknowledgement

The authors thank Cummins India Limited for the support provided.

## References

1. Astbury GR. A review of the properties and hazards of some alternative fuels. *Process Safety Environ Protect* 2008; 86(6): 397–414.
2. Rakopoulos CD and Michos CN. Development and validation of a multi-zone combustion model for performance and nitric oxide formation in syngas fueled spark ignition engine. *Energy Convers Manage* 2008; 49(10): 2924–2938.
3. Heywood JB. *Internal combustion engine fundamentals*. Singapore: McGraw-Hill, 1988, 2002.
4. Yang S and Reitz RD. Improved combustion submodels for modeling gasoline engines with the level set g equation and detailed chemical kinetics. *Proc IMechE, Part D: J Automobile Engineering* 2009; 223(5): 703–726.
5. Chiodi M. *An innovative 3D-CFD-approach towards virtual development of internal combustion engines*. New York: Springer, 2011.
6. Verhelst S and Sheppard CGW. Multi-zone thermodynamic modeling of spark-ignition engine combustion-an overview. *Energy Convers Manage* 2009; 50(5): 1326–1335.
7. Heywood JB, Higgins JM, Watts PA, et al. *Development and use of a cycle simulation to predict SI engine efficiency and NOx emissions*. vol. 790291, Warrendale, PA: Society of Automotive Engineers, 1979.
8. Giansetti P, Colin G, Higelin P, et al. Residual gas fraction measurement and computation. *Int J Engine Res* 2007; 8(4): 347–364.
9. Soyulu S. Prediction of knock limited operating conditions of a natural gas engine. *Energy Convers Manage* 2005; 46(1): 121–138.
10. Lounici MS, Loubar K, Balistrrou M, et al. Investigation on heat transfer evaluation for a more

- efficient two-zone combustion model in the case of natural gas SI engines. *Appl Therm Eng* 2011; 31(2-3): 319–328.
11. Rivas-Renault M, Higelin-Prisme P, Caillol-Prisme C, et al. Validation and application of a new 0d flame/wall interaction sub model for SI engines. *SAE Int J Engines* 2012; 5(3): 718–733.
  12. Malbec LM, Le Berr F, Richard S, et al. Modeling turbocharged spark-ignition engines: towards predictive real time simulators. *SAE Technical Paper* 2009, p. 01 0675.
  13. Le Solliec G, Le Berr F, Colin G, et al. Engine control of a downsized spark ignited engine: from simulation to vehicle. *Oil Gas Sci Technol* 2007; 62(4): 555–572.
  14. Richard S, Bougrine S, Font G, et al. On the reduction of a 3d CFD combustion model to build a physical 0d model for simulating heat release, knock and pollutants in si engines. *Oil Gas Sci Technol* 2009; 64(3): 223–242.
  15. Dasappa S, Sridhar G, Sridhar HV, et al. Producer gas engines—proponent of clean energy technology. In: *Proceedings of 15th european biomass conference and exhibition—from research to market deployment—biomass for energy, industry and climate protection*, Berlin, Germany. 2007, pp. 976–981.
  16. Glassman I. *Combustion*. Academic Press, 1996.
  17. Kuo KK. *Principles of combustion*. New Jersey: John Wiley & Sons, 2005.
  18. Sonntag RE, Borgnakke C, Van Wylen GJ, et al. *Fundamentals of thermodynamics*. New York: Wiley, 1998.
  19. Turns SR. *An introduction to combustion: concepts and applications*. vol. 10. New York: McGraw-hill, 1996.
  20. Karim GA, Wierzbka I and Al-Alousi Y. Methane-hydrogen mixtures as fuels. *Int J Hydrogen Energy* 1996; 21(7): 625–631.
  21. Bell SR and Gupta M. Extension of the lean operating limit for natural gas fueling of a spark ignited engine using hydrogen blending. *Combust Sci Technol* 1997; 123(1–6): 23–48.
  22. Roger IR. Natural gas/hydrogen mixtures for low noxious emissions. *J Scient Ind Res* 2003; 62(1–2): 64–70.
  23. Serrano C, Hernandez JJ, Mandilas C, et al. Laminar burning behaviour of biomass gasification-derived producer gas. *Int J Hydrogen Energy* 2008; 33(2): 851–862.
  24. Hernandez JJ, Lapuerta M, Serrano C, et al. Estimation of the laminar flame speed of producer gas from biomass gasification. *Energy Fuels* 2005; 19(5): 2172–2178.
  25. Bechtold JK and Matalon M. Hydrodynamic and diffusion effects on the stability of spherically expanding flames. *Combust Flame* 1987; 67(1): 77–90.
  26. Gillespie L, Lawes M, Sheppard CGW, et al. Aspects of laminar and turbulent burning velocity relevant to SI engines. *SAE Trans* 2000; 109(3): 13–33.
  27. Galindo J, Climent H, Plá B, et al. Correlations for Wiebe function parameters for combustion simulation in two-stroke small engines. *Appl Therm Eng* 2011; 31(6–7): 1190–1199.
  28. Sridhar G, Paul PJ and Mukunda HS. Biomass derived producer gas as a reciprocating engine fuel—an experimental analysis. *Biomass Bioenergy* 2001; 21(1): 61–72.
  29. Sridhar G, Sridhar HV, Dasappa S, et al. Development of producer gas engines. *Proc IMechE, Part D: J Automobile Engineering* 2005; 219(3): 423–438.
  30. Dasappa S, Sridhar HV and Indrajit M. Experiments on and thermodynamic analysis of a turbocharged engine with producer gas as fuel. *Proc IMechE, Part C: J Mechanical Engineering Science* 2011.
  31. Dasappa S, Sridhar G and Paul PJ. Adaptation of small capacity natural gas engine for producer gas operation. *Proc IMechE, Part C: J Mechanical Engineering Science* 2011.
  32. Sridhar G, Paul PJ and Mukunda HS. Zero-dimensional modeling of a producer gas-based reciprocating engine. *Proc IMechE, Part A: J Power and Energy* 2006; 220(8): 923–931.
  33. Rakopoulos CD, Michos CN and Giakoumis EG. Availability analysis of a syngas fueled spark ignition engine using a multi-zone combustion model. *Energy* 2008; 33(9): 1378–1398.
  34. Stone CR and Green-Armytage DI. Comparison of methods for the calculation of mass fraction burnt from engine pressure time diagrams. *Proc IMechE, Part D: J Transport Engineering* 1987; 201(14): 61–67.
  35. Caton JA. Operating characteristics of a spark-ignition engines using the second law of thermodynamics: effects of speed and load. *SAE Technical Paper* 2000-01-0952, 2000.
  36. Gallo WLR and Milanez LF. Society of Automotive Engineers. Exergetic analysis of ethanol and gasoline fueled engines. Technical Report. Society of Automotive Engineers, Warrendale, PA, 1992.
  37. Ramos JI. Comparisons between thermodynamic and one-dimensional combustion models of spark-ignition engines. *Appl Math Model* 1986; 10(6): 409–422.
  38. Ibrahim A and Bari S. Optimization of a natural gas si engine employing egr strategy using a two-zone combustion model. *Fuel* 2008; 87(10–11): 1824–1834.
  39. Kakaee AH, Shojaeefard MH and Zareei J. Sensitivity and effect of ignition timing on the performance of a spark ignition engine: an experimental and modeling study. *J Combust* 2011; 2011: 678719.
  40. Mustafi NN and Raine RR. Application of a spark ignition engine simulation tool for alternative fuels. *J Eng Gas Turb Power* 2008; 130: 012804.
  41. Rao SG. Experiments and modelling studies of producer gas based spark-ignited reciprocating engines. PhD thesis. Indian Institute of Science, 2003.
  42. Ferguson CR and Kirkpatrick AT. *Internal combustion engines: applied thermosciences*. 2nd edn. New York: Wiley, 2000.
  43. Watson N and Janota MS. *Turbocharging the internal combustion engine*. London: MacMillan, 1982.
  44. Chevalier A, Muller M and Hendricks E. On the validity of mean value engine models during transient operation. *SAE Trans* 2000; 109(3): 1571–1592.
  45. Stotsky AA. *Automotive engines: control, estimation, statistical detection*. New York: Springer Verlag, 2009.
  46. Annand WJD and Roe GE. *Gas flow in the internal combustion engine: power, performance, emission control, and silencing*. Sparkford, Somerset, UK: GT Foulis, 1974.
  47. Oppenheim AK. *Combustion in piston engines: technology, evolution, diagnosis, and control*. New York: Springer Verlag, 2004.
  48. Devore JL. *Probability and statistics for engineering and the sciences*. Boston: Duxbury Press, 2011.

49. Ghojel J. Review of the development and applications of the wiebe function: A tribute to the contribution of ivan wiebe to engine research. *Int J Engine Res* 2010; 11(4): 297–312.
50. Borg JM and Alkidas AC. On the application of wiebe functions to simulate normal and knocking spark-ignition combustion. *Int J Vehicle Design* 2009; 49(1): 52–69.
51. Shiao Y and Moskwa JJ. Cylinder pressure and combustion heat release estimation for si engine diagnostics using nonlinear sliding observers. *IEEE Trans Contr Sys Technol* 1995; 3(1): 70–78.
52. Pipitone E. A comparison between combustion phase indicators for optimal spark timing. *J Eng Gas Turb Power* 2008; 130: 052808.
53. Abraham J and Magi V. Modeling radiant heat loss characteristics in a diesel engine. SAE Technical Paper 970888, 1997.
54. Annand WJD. Heat transfer in the cylinders of reciprocating internal combustion engines. *Proc Inst Mech Eng* 1963; 177(1): 973–996.
55. Woschni G. A universally applicable equation for the instantaneous heat transfer coefficient in the internal combustion engine. SAE Paper, 670931, 1967.
56. Hohenberg GF. Advanced approaches for heat transfer calculations. Technical report, Society of Automotive Engineers. Warrendale, PA, 1979.
57. Tahtouh T, Halter F, Mounaïm-Rousselle C, et al. Experimental investigation of the initial stages of flame propagation in a spark-ignition engine: effects of fuel, hydrogen addition and nitrogen dilution. *SAE Int J Eng* 2010; 3(2): 1–19.
58. Wang J, Huang Z, Miao H, et al. Characteristics of direct injection combustion fuelled by natural gas-hydrogen mixtures using a constant volume vessel. *Int J Hydrogen Energy* 2008; 33(7): 1947–1956.
59. D'Andrea T, Henshaw PF and Ting DSK. The addition of hydrogen to a gasoline-fuelled si engine. *Int J Hydrogen Energy* 2004; 29(14): 1541–1552.
60. Shivapuji AM and Dasappa S. Experimental studies on multi-cylinder natural gas engine fueled with producer gas. In: *Proceedings of 19th European biomass conference and exhibition from research to industry and markets*, Berlin, Germany. 2011, pp.974–980.
61. Ma F, Wang Y, Wang J, et al. Effects of combustion phasing, combustion duration, and their cyclic variations on sparkignition (si) engine efficiency. *Energy Fuels* 2008; 22(5): 3022–3028.
62. Shudo T. Improving thermal efficiency by reducing cooling losses in hydrogen combustion engines. *Int J Hydrogen Energy* 2007; 32(17): 4285–4293.
63. Lyford-Pike EJ and Heywood JB. Thermal boundary layer thickness in the cylinder of a spark-ignition engine. *Int J Heat Mass Transfer* 1984; 27(10): 1873–1878.
64. Tazerout M, Le Corre O and Ramesh A. A new method to determine the start and end of combustion in an internal combustion engine using entropy changes. *Int J Thermodyn* 2010; 3(2): 49–55.

## Appendix

### Notation

$a$	efficiency factor
$B$	linear dimension (bore diameter)
$c$	speed of sound
$e$	exit conditions
$h_{c,g}$	convective heat transfer coefficient
$i$	inlet conditions
$k$	thermal conductivity
$m$	shape factor
$\dot{m}$	mass flow rate
$\dot{q}$	convective heat flux
$P$	cylinder pressure
$Q$	heat transfer
$Q_{HV_f}$	fuel lower heating value
$Q_{HV_i}$	specie lower heating value
$\bar{S}_p$	mean piston speed
$\bar{T}_g$	mean gas temperature
$T_{w,g}$	wall temperature
$V$	cylinder volume
$X_i$	specie mass fraction
$\theta$	crank angle
$\gamma$	polytropic index
$\eta_c$	combustion efficiency
$\mu$	dynamic viscosity
$\rho$	density